Neutron yield of thick ^{12}C and ^{13}C targets with 20 and 30 MeV deuterons

G. Lhersonneau, T. Malkiewicz, M. Fadil, D. Gorelov, P. Jones, P.Z. Ngcobo,
J. Sorri, W.H. Trzaska

HAL Id: in2p3-01403247

http://hal.in2p3.fr/in2p3-01403247

Submitted on 25 Nov 2016

Neutron yield of thick ^{12}C and ^{13}C targets with 20 and 30 MeV deuterons

G. Lhersonneau[1], T. Malkiewicz[2], M. Fadil[1], D. Gorelov[3], P. Jones[4], P.Z. Ngcobo[4], J. Sorri[3], and W.H. Trzaska[3]

1 GANIL, Bld H. Becquerel, B.P. 55027, 14076 Caen Cedex 05, France
2 CSC - IT Center for Science Ltd., P.O.Box 405, Keilaranta 14, 02101 Espoo, Finland
3 Department of Physics, University of Jyvaskyla, P.O.Box 35, 40351-Jyvaskyla, Finland
4 iThemba Laboratory for Accelerator Based Science, P.O.Box 722, Somerset West 7129, Western Cape, South Africa

Abstract. The neutron yield of thick targets of carbon, natural and enriched in ^{13}C, bombarded by deuterons of 20 and 30 MeV has been measured by the activation method. The gain with respect to a ^{12}C target is the same as with protons beams. The yield ratio is about 1.2 only and hardly can justify the use of a ^{13}C target with deuteron beams. The data, apart from being of interest for the design of facilities where secondary neutron beams are used, provide a test case for calculations where both beam and target have a weakly-bound neutron. The MCNPx code version 2.6.0, despite failing to reproduce some details of the experimental distributions, describes their global properties fairly well, especially the relative yields of the ^{12}C and ^{13}C targets.

1 Introduction

The knowledge of reactions induced by fast neutron beams has grown in interest since the advent of accelerators capable of delivering high-current proton or deuteron beams in the intermediate energy regime. Impinging and subsequent absorption of charged-particle beams in thick targets is able to generate neutrons of several tens of MeV with a yield approaching 1% of the beam particle current. A necessarily too short list of applications is mentioned below.

ISOLDE at CERN [1] has been for quite some time producing intense flux of fast neutrons generated by the interaction of 1.4 GeV proton beams on a tungsten converter target. These neutrons are mostly used for nuclear studies of very neutron-rich nuclei produced by fission of massive targets. It is worth to note the plan at CERN to use the ^{9}Be(n,α)^{6}He reaction in order to generate beams of neutrinos [2].

At much lower primary beam energy the IGISOL ion-guide on-line mass separator, at Jyväskylä, Finland, is also devoted to nuclear physics. It has recently been connected to a new high-current 30 MeV cyclotron. Neutron yields close to 10^{12}/s are expected using protons on a beryllium

Send offprint requests to: tomasz.malkiewicz@csc.fi

target [3].

As a first step to the very ambitious European project EURISOL [4] the SPIRAL2 facility at GANIL, Caen, France is based on 40 MeV deuteron beams delivered by a new 5 mA linac driver [5]. We note that the first application to be operational at SPIRAL2 will be a dedicated neutron facility, Neutrons for Science [6,7], offering a variety of applications to measurements of cross-sections, nuclide production and studying medical and technological issues. Among them is the interaction of secondary neutrons in human cells, in connection with radiotherapy with charged particles, for instance proton or ^{12}C beams. The ARCHADE facility for cancer treatment [8] is foreseen to be implemented at the GANIL site. Another application is the production of radio-isotopes. Their production with intense neutron beams may be in some cases an interesting alternative to neutron capture or fission with thermal neutrons at high-flux reactors. It has been reported recently that an accelerator with the same characteristics as the linac driver for SPIRAL2 at GANIL would generate enough neutrons via d + ^{12}C to be able to supply Japan for its demand on the ^{99}Tc medical isotope produced via ^{100}Mo(n,2n)^{99}Mo and its subsequent β-decay [9].

Better knowledge of reactions of intermediate-energy neutrons with matter is very important for the design of facilities where secondary neutrons will be produced in

large amounts. As an example, the IFMIF facility in Japan [10] is being built to test the behaviour of the materials to be used at the ITER fusion test reactor [11] under intense neutron flux. Neutron cross-section data are compiled by the National Nuclear Data Center (NNDC) [12]. Evaluated data (ENDF) mostly cover a range up to 20 MeV while there are rather few data listed at higher energies in the experimental (EXFOR) database. More experiments should be carried out with higher-energy neutrons to benchmark the reaction codes and provide a guidance for applications.

Activation measurements can be used to obtain the envelope of a continuous neutron spectrum or of a cross-section without resonances. The radioactivity of the residual nucleus gives access to the integral overlap of these quantities. The measurement requires a set of overlaps, where one of the quantities is known and the unknown one will be obtained by iterative unfolding of the overlaps. A cross-section measurement can be carried out by irradiating foils of a material suitable to measure the neutron spectrum together with a target of the nucleus under study. Our group has recently completed such a test and intends to measure the cross-section for ^{18}O(n,α)^{15}C, as part of a scheme to be investigated for a post-accelerated ^{15}C beam at SPIRAL2.

The present work reports on neutron measurements in the context of Radioactive Beam Facilities, in which neutron-induced fission is the reaction leading to neutron-rich nuclei. Several authors of this work have been involved in experiments to search for the best neutron production scheme. The first measurements were carried out in the frame of the original version of the SPES project at Legnaro, Italy, [13], based on proton beams and a carbon target enriched in ^{13}C as the neutron production target [14,15]. Later on, the neutron yields of carbon and heavy-water targets with 40 and 55 MeV deuteron beams have been tested [16,17] and isotope yields in neutron-induced fission of natural uranium have been measured [18] in the context of SPIRAL2. A review of these works is given in [19]. The present work is carried out to investigate whether a ^{13}C target will be rewarding with deuteron beams. There exists to our knowledge only a single measurement made by Donzella et al. at LNS, Catania, Italy [20], the beam being 40 MeV deuterons and it is only a neutron spectrum at 30° from the beam axis.

2 Experiment

The experiments have been carried out at the K-130 cyclotron of the Physics Department of the University of Jyväskylä. The target container and current measurement device were the same as in the latest of our previous works. A scheme of the target system is shown in Fig.1 of Ref. [15]. The targets were a natural carbon powder (density 1.70 g/cm^3) and a powder enriched to 82% in ^{13}C (density 1.76 g/cm^3). Their thickness was sufficient to stop

the beams. The entrance window was made of 0.5 mm aluminum. The target worked as a Faraday cup, allowing the collected charge to be constantly monitored. The nominal accuracy of the charge integrator [21] was better than 1%. Leaks from the target to the integrator have been previously estimated using calibrated intensity sources. The accuracy of the system has been estimated to be better than 3%. With proton beams the gain, i.e. the ratio of neutron yield of ^{13}C to ^{12}C targets, in short y(^{13}C)/y(^{12}C), was the strongest at the lowest proton energies [14,15]. We therefore decided to measure the relative yields of ^{13}C and ^{12}C targets at deuteron energies (E$_d$) of 20 MeV and 30 MeV.

Stacks of Al, Ni, Co, In and Bi foils (Bi at E$_d$ = 30 MeV only) have been submitted to the neutrons emerging from the target. The foils were all squares of 2.5 by 2.5 cm of 0.1 cm thickness obtained commercially [22]. The foils were placed at θ = 0°, 20°, 40°, 60° and 90° from the beam axis. The respective distances from the center of the target to the middle of the foil stack were 23.5, 19.5, 19.5, 11.5 and 8.5 cm. Due to the finite size of the foils, the nominal angle of 0° was actually 2.3^o, which is the mean θ value of the neutrons hitting the foil. The irradiations with 20 MeV deuterons lasted for about 10 hours, and 8 hours at E$_d$= 30 MeV. The currents were remarkably constant during each measurement and ranged from 18 nA to 7 nA.

After irradiation, the foil stacks were split as Al-Ni and Co-In(-Bi) stacks and counted with 2 coaxial Ge-detectors, one being a 25% efficiency coaxial-Ge (GMX) we used previously, and the other one being a GASP Ge-detector borrowed from the JUROGAMII array at JYFL. Two days after the last irradiation was over, the later was replaced with a PopTop with electrical cooling in a closer geometry in order to count the ^{58}Co long-lived activity. The peak efficiencies at the 1368.6 keV γ-ray of ^{24}Na activity produced in Al-foils via (n,α) were 0.31% (GMX), 0.66% (GASP) and 0.89% (PopTop), respectively. Countings started typically 10 minutes after the end of irradiations. Their duration was adapted to the half-lives of the activation products. Each foil was counted at least twice, else three times for safety and checks of consistency. The whole counting was ended 10 days after the last irradiation. Examples of spectra are shown in figures 1 and 2. Lines other than the natural background and a contamination of the detector cap with ^{152}Eu are commented in the captions.

3 Analysis

The method is reviewed here. More details are given in Refs. [16,17].

The foils, placed at an angle θ to the beam axis, cut a small solid angle Ω defined by their area and distance to the converter target. The variation of the neutron flux over the foil volume being neglected, the spectrum $n_\theta(E)$
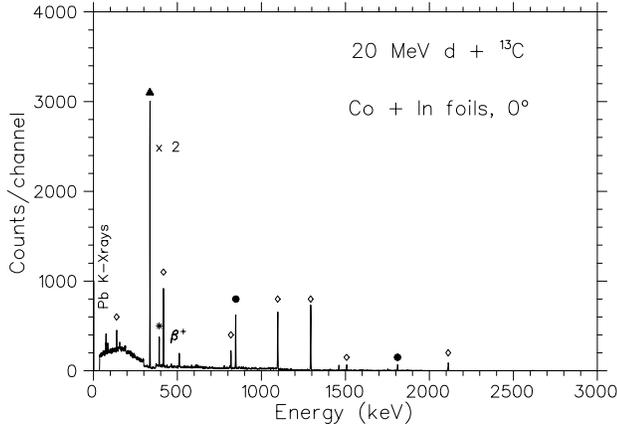
Fig. 1. Spectrum recorded 30 minutes after the end of irradiation during 20 minutes. Lines marked with diamonds are due to ^{115}In(n,γ). The 391.7 keV line (star) is from ^{113}In(n,n'). The lines at 336.2 keV (^{115}In(n,n'), triangle), 846.8 and 1810.7 keV (^{59}Co(n,α)^{56}Mn, full circles) are included in the analysis.
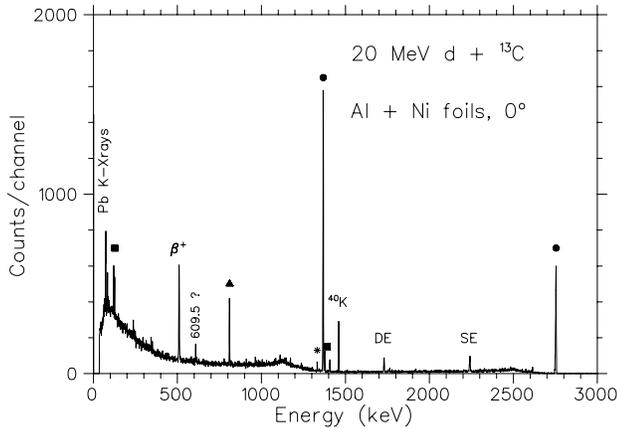

Fig. 2. Spectrum recorded 5 hours after the end of the irradiation for a duration of 40 minutes. The lines at 810.8 keV (^{58}Ni(n,p)^{58}Co, triangle), the 1368.6 and 2754.0 keV (^{27}Al(n,a)^{24}Na, circles) and the 127.2 and 1377.6 keV (^{58}Ni(n,2n)^{57}Ni, squares) have been used in the analysis. Other lines are an unidentified 609.5 keV, the 1332.5 keV (^{60}Ni(n,p)^{60}Co^m, star) and the single (SE) and double (DE) - escape peaks of the 2754.0 keV.

is proportional to the double-differential distribution of the neutron flux ϕ via

$$n_\theta(E) = \frac{\partial^2 \phi(\theta, E)}{\partial E \, \partial \Omega} \; \Omega.$$

In the following, the index θ is dropped since the context is obvious. The overlap integral,

$$<\sigma.n> = \int \sigma(E) \, n(E) \, dE$$

where $\sigma(E)$ is the cross-section of the reaction, is directly extracted from the area of the γ-ray peaks. The spectrum

is obtained after unfolding a set of such integrals for different reactions. The cross-sections were taken from the experimental and evaluated data bases EXFOR and ENDF of NNDC [12]. A plot of those used in this work is shown in Fig.3 of Ref. [15].

The analysis begins with a data reduction to get the overlap integrals for each reaction. This starts with a step to obtain the number of decays occuring during the counting time from the peak area, detection efficiency ε_γ and decay branching b_γ of the main γ-rays in the decay of the product nucleus. The detector efficiency is described as the product of the efficiency for a point source and of a calculated correction factor to account for the volume of the foils and absorption in the various layers of the stack. We apologize for the unlucky truncation in Ref. [18] of the expression for the mean-absorption length of γ-rays in the Ge crystal as $1/\mu$, μ being the linear absorption coefficient [23]. [1]

The point-source efficiency was obtained from measurements with ^{137}Cs, ^{152}Eu and ^{60}Co standard sources. In addition, the ^{24}Na activity produced during the irradiations allowed to extend the energy range of the efficiency curve beyond 1408 keV by comparing the areas of the 1368 and 2754 keV peaks. The adopted error on the efficiency is composed of the quoted uncertainty on the source strengths (5%) and the r.m.s. relative deviation of experimental and fitted values (another 5% typically). The error on the calculated correction factor is supposed to be negligible.

The second step of data reduction links the number of decays with the experimental overlap integral $<\sigma.n>$. Firstly, the production rate of the residual nucleus is computed as the number of decays corrected for a 'time factor' depending only on the half-life of the decaying nucleus and the times of irradiation and of counting. The dead time was taken from the active and real times of the acquisition system. Then, subsequent normalisations for the number of target nuclei per unit area in the foil, the solid angle of the foil Ω and the number of projectiles per second leads to $<\sigma.n>$. Systematical errors on the overlaps are the error on the beam current reading and ε_γ. They contribute to a 8% hard-core error. Yet, they act on all values in the same way and do not need to be considered in a comparison of relative values. Individual errors other than those due to weak statistics are small. The small uncertainty on Ω has been calculated with an error of 3 mm on the distance along the beam axis. Errors on foil weights are lower than 0.1%. Errors on b_γ are usually small too and do not impact the result.

---

[1] The value for a parallel beam impinging on a detector of length L along its symmetry axis is

$$\overline{x} = \frac{\int x \, e^{-\mu x} \, dx}{\int e^{-\mu x} dx} = \frac{1}{\mu} \, \frac{1 - e^{-\mu L} - \mu L \, e^{-\mu L}}{1 - e^{-\mu L}}$$

After data reduction, the final stage of the analysis is the unfolding of the overlap integrals. It consists of searching by iterations for the best agreement between the overlap integrals calculated with a trial neutron spectrum and the experimental set. The spectrum $n(E)$ is obtained by interpolation between a set of values at selected energies being varied during the iterations. The procedure is repeated at each angle independently.

It seemed necessary to use at least 5 variable points, $n(E_k)$, plus a fixed point to end the spectrum slightly above the beam energy. Weak statistics prevented the use of the Bi(n,4n) reaction, except at the smallest angles at E_d= 30 MeV. In absence of enough degrees of freedom, the lowest χ^2 led to a spectrum shape in poor agreement with the expected one. The adopted $n(E_k)$ set was therefore obtained by applying constrains to the spectrum shape. The guide for the spectrum shape was the spectrum measured at the deuteron energy of 40 MeV for the ^{12}C target [16] compressed in energy. It was further required to ask for a smooth variation of the $n(E_k)$ parameters obtained for different θ values, and that the average discrepancy of calculated and experimental overlap integrals remained within twice the error bars made of the experimental errors without the 8% hard-core error. The adjustment modified the integrals of spectra only to a small extent. The average ratio, considering all beam energies, angles and targets, of integrals with/without constrains was 1.08. It could be appropriate to regard this 8% change as a measure of the accuracy of relative flux values for the ^{12}C and ^{13}C targets. For the absolute values this 8% bound to the unfolding must be added to the other 8% systematical error. Moreover, cross-sections used for the unfolding are reported with errors of about 10%. It is difficult to estimate how much these may affect the result without repeating the analysis by changing each of the cross-sections one by one. If there are n of them, a tentative estimate is $10\%/\sqrt{n}$. All in all, the error on the neutron flux per deuteron may be about 15%.

4 Results

The overlap integrals are shown in table 1. The errors shown do not include the contributions of the 8% hard-core error acting in a coherent way on all values. The double-differential distributions are shown plotted versus neutron energy and angle to the beam axis in figures 3, 4, 5 and 6.

The angular distributions of all neutrons above 1 MeV are shown in figure 7. The interpolation uses the $\cos(\theta)$ variable in order to create a flatter behaviour at 0 degree. The angles at half maximum are 18° (^{12}C, 20 MeV), 19° (^{13}C at 20 MeV) and 16° at E_d= 30 MeV for both targets.

While a detailed discussion of spectral shapes is of little relevance due to the method of analysis, it may still be worth to comment the gross properties of the data, i.e.

Table 1. Experimental overlap integrals in mb/sr, normalised for 100 deuterons. Production reactions are indicated as (E_d, target). A blank space indicates there was no foil, while a hyphen indicates that the peaks were too weak to be exploited.

$\theta = \quad 0^o$	(20, ^{12}C)	(20, ^{13}C)	(30, ^{12}C)	(30, ^{13}C)
Al(α)^{24}Na	22.7(9)	26.0(14)	81.1(55)	93.6(43)
Co(2n)^{58}Co	65.7(35)	75.8(38)	426(28)	464(45)
Co(α)^{56}Mn	5.07(32)	5.53(39)	20.6(9)	21.4(13)
Ni(2n)^{57}Ni	2.64(17)	3.61(25)	25.3(14)	31.6(35)
Ni(p)^{58}Co	242(9)	229(26)	526(23)	660(25)
In(n')^{115}In	111(6)	131(11)	235(16)	252(18)
Bi(4n)^{206}Bi			8.08(99)	18.3(21)

$\theta = 20^o$	(20, ^{12}C)	(20, ^{13}C)	(30, ^{12}C)	(30, ^{13}C)
Al(α)^{24}Na	6.94(28)	6.87(67)	17.0(16)	20.3(81)
Co(2n)^{58}Co	20.0(11)	24.9(21)	90.7(72)	84.2(101)
Co(α)^{56}Mn	1.55(8)	1.52(12)	4.47(20)	4.02(28)
Ni(2n)^{57}Ni	1.01(9)	1.51(11)	6.22(48)	7.60(59)
Ni(p)^{58}Co	80.4(32)	86.5(53)	160(8)	185(8)
In(n')^{115}In	44.9(23)	54.4(27)	86.3(43)	106(7)
Bi(4n)^{206}Bi			1.58(19)	6.70(94)

$\theta = 40^o$	(20, ^{12}C)	(20, ^{13}C)	(30, ^{12}C)	(30, ^{13}C)
Al(α)^{24}Na	1.71(10)	2.09(15)	5.48(36)	6.66(37)
Co(2n)^{58}Co	4.40(41)	6.71(89)	25.2(25)	27.0(30)
Co(α)^{56}Mn	0.33(2)	0.49(6)	1.20(9)	1.38(36)
Ni(2n)^{57}Ni	0.18(4)	0.22(5)	1.57(18)	2.36(20)
Ni(p)^{58}Co	29.0(12)	33.3(20)	60.5(72)	82.7(43)
In(n')^{115}In	21.0(11)	25.8(17)	36.8(22)	54.1(40)
Bi(4n)^{206}Bi			-	2.00(79)

$\theta = 60^o$	(20, ^{12}C)	(20, ^{13}C)	(30, ^{12}C)	(30, ^{13}C)
Al(α)^{24}Na		0.95(5)	2.48(12)	3.04(14)
Co(2n)^{58}Co		2.67(35)	5.75(55)	11.2(10)
Co(α)^{56}Mn		0.22(4)	0.32(6)	0.72(5)
Ni(2n)^{57}Ni		0.13(5)	0.60(10)	1.07(21)
Ni(p)^{58}Co		18.6(10)	34.6(18)	46.5(24)
In(n')^{115}In		15.8(12)	25.7(16)	36.5(25)

$\theta = 90^o$	(20, ^{12}C)	(20, ^{13}C)	(30, ^{12}C)	(30, ^{13}C)
Al(α)^{24}Na	0.36(2)	0.51(3)	1.34	1.69(12
Co(2n)^{58}Co	0.68(7)	1.13(17)	2.06(17)	4.85(45)
Co(α)^{56}Mn	0.08(2)	0.12(2)	0.18(2)	0.37(3)
Ni(2n)^{57}Ni	0.03(2)	0.12(2)	0.30(3)	0.38(5)
Ni(p)^{58}Co	10.7(7)	13.0(9)	23.7(17)	32.6(23)
In(n')^{115}In	10.9(8)	13.0(10)	20.8(15)	29.2(21)

the integral of the spectra and the median energy (half of the neutrons have a lower - or higher - energy). Flux and median-energy values are shown in table 2. The flux per deuteron indicates modest gains factors of 1.17 (20 MeV) and 1.18 (30 MeV) with respect to ^{12}C. When raising the neutron energy threshold to 4 MeV, the corresponding factors decrease to 1.07 and 1.14, respectively. The extra neutrons are therefore mostly located at low energy. This is also shown by the median energy, lower for ^{13}C than for ^{12}C. The different bindings of the last neutron,
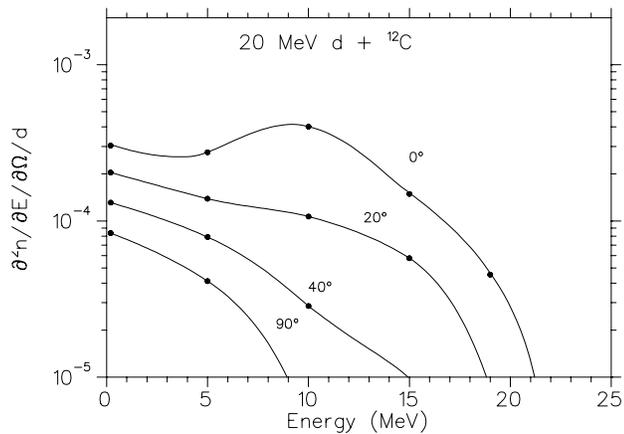
Fig. 3. Double-differential distribution of neutrons per MeV, per sr and per deuteron for the 20 MeV d + ^{12}C reaction, versus energy and at various angles from beam axis. Dots mark the $n(E_k)$ parameters of the unfolding.
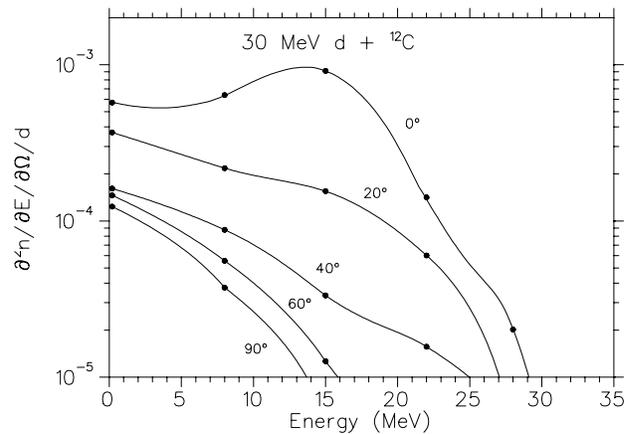

Fig. 5. Double-differential distribution of neutrons per MeV, per sr and per deuteron for the 30 MeV d + ^{12}C reaction, versus energy and at various angles from beam axis. Dots mark the $n(E_k)$ parameters of the unfolding.

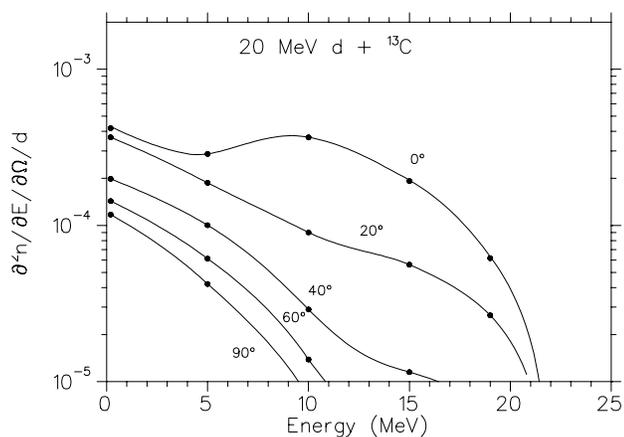**Fig. 4.** Double-differential distribution of neutrons per MeV, per sr and per deuteron for the 20 MeV d + ^{13}C reaction, versus energy and at various angles from beam axis. Dots mark the $n(E_k)$ parameters of the unfolding.

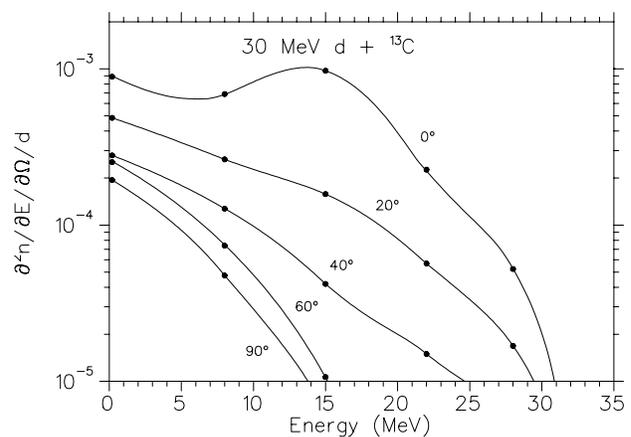**Fig. 6.** Double-differential distribution of neutrons per MeV, per sr and per deuteron for the 30 MeV d + ^{13}C reaction, versus energy and at various angles from beam axis. Dots mark the $n(E_k)$ parameters of the unfolding.

i.e. $S_n(^{12}$C$)$= 18.7 MeV, $S_n(^{13}$C$)$= 4.9 MeV [12], explain that deuterons near the end of their range can release a neutron from the ^{13}C target but not anymore from the ^{12}C target. The median angle of neutrons above 1 MeV is rather an indication of a trend than a well-defined value due to the interpolation over wide intervals up to 90°. A slightly flatter becoming angular distribution with increasing energy is in agreement with kinematics.

5 Discussion

5.1 Comparison with other measurements

Neutron yields for p and d reactions on ^{12}C and ^{13}C targets are shown in figure 8. The neutrons are included if their energy is above 4 MeV and they are emitted at an
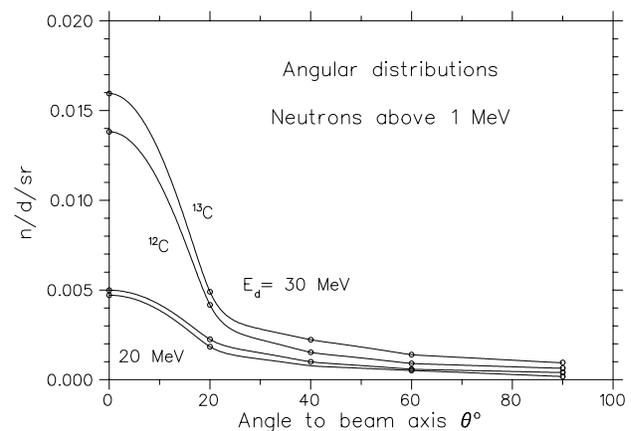

Fig. 7. Angular distributions of neutrons above 1 MeV.

Table 2. Neutron flux for 100 deuterons $(n/100\,d)$ and median energy E_{med} calculated with an energy threshold of 1 MeV and $\theta < 30^o$ and the median angle θ_{med}.

E_d (MeV)	Target	(n/100 d)	E_{med} (MeV)	θ_{med} (^{o})
20	^{12}C	0.192	7.2	39
	^{13}C	0.225	5.9	39
30	^{12}C	0.490	10.0	33
	^{13}C	0.578	9.1	37

angle not larger than 30° from the beam axis. Lines for proton beams are only to guide the eye, while the one for d + ^{12}C is an empirical fit with the deuteron energy to the power 2.5 which has been used to estimate the contribution of neutrons produced in the entrance window, which is discussed at the end of this subsection. The integral values obtained in this work are listed in table 3.

The agreement of our points for the ^{12}C target with the interpolation from the literature data is good. It is, however, worth to note that the three points measured by us, either in the present experiment at E_d= 20 and 30 MeV or at 40 MeV [16] are slightly below the interpolation of the Time-of-Flight measurements.

Donzella et al. [20] measured a neutron spectrum for 40 MeV deuterons on a ^{13}C target. The spectrum was recorded at 30° from the beam axis with a new type of neutron detector, in which the neutron energy is reconstructed from the analysis of the kinematics of the recoil proton. They reported a differential yield of $2.0\,10^{-3}$ neutrons of energy larger than 6 MeV per sr and per deuteron. Under the same conditions, the corresponding value for 42.5 MeV deuterons [16] (of which 2.5 MeV were absorbed in the entrance window) on ^{12}C is $3.7\,10^{-3}$ n/sr/d (with 15% error). It may become smaller at 40 MeV (about 0.86 times) to become $3.2\,10^{-3}$ n/sr/d. Whatever should the gain with ^{13}C be, there is a discrepancy of at least a factor of 1.7, see also table 3. The reason for it is not established but possibly could be an overestimate of the efficiency of their new detector.

Table 4 compares the flux with proton and deuteron beams at same projectile energy as it can be read from Fig. 8. The differences y(^{13}C) - y(^{12}C) at same beam energy are almost the same, being slighly larger for the deuteron beam. The ratio y(^{13}C)/y(^{12}C) is large for proton beams (i.e. quasi infinite at E_p= 20 MeV and 5.3 at E_p= 30 MeV) but for deuterons beams, as it results from this work, it hardly would exceed 1.2. The main contribution to the yield is the deuteron break-up and the target modifies it only marginally.

The observed gains could have been larger and more different from each other if the entrance aluminum win-
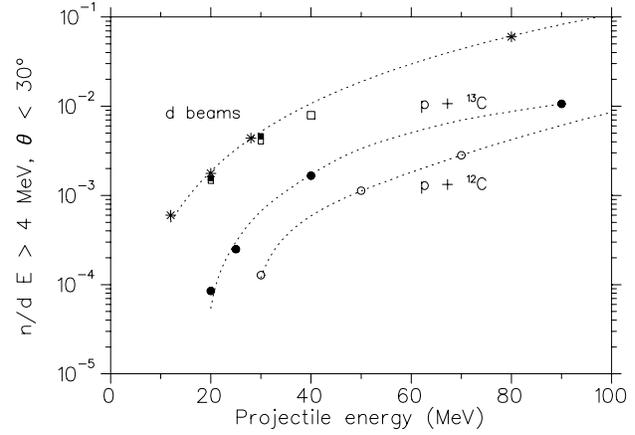

Fig. 8. A comparison of neutron yields for p and d reactions on ^{12}C and ^{13}C targets. Squares (open for ^{12}C, closed for ^{13}C) are from the present activation measurements and Ref. [16] for ^{12}C at 40 MeV. Closed circles are our earlier measurents for proton beams at 20, 25, and 40 MeV [15]. This reference also contains references for the measurement at 80 MeV, the TOF measurements for d + ^{12}C (stars) and the TOF measurements for p + ^{12}C (open circles).

Table 3. Neutron flux above 4 MeV and for $\theta < 30^o$, $(n/100\,d)$, and the integral above 6 MeV of the spectrum per steradian interpolated at $\theta= 30^o$, $(n/sr/100\,d)_{30}$, both for 100 incident deuterons. The last column is to allow for a comparison with Ref. [20].

E_d (MeV)	Target	(n/100 d)	$(n/sr/100\ d)_{30}$
20	^{12}C	0.146	0.064
	^{13}C	0.156	0.069
30	^{12}C	0.403	0.165
	^{13}C	0.460	0.192
42.5	^{12}C	0.685	0.372 [16]
40	^{13}C		0.20 [20]

Table 4. Neutron yields of ^{12}C and ^{13}C targets with proton and deuteron beams, as in Fig.8 and their differences and ratios.

E (MeV)	Beam	^{12}C	^{13}C	Difference	Ratio
20	d	0.146	0.156	0.010	1.07
20	p	0.0	0.0085	0.0085	∞
30	d	0.403	0.460	0.057	1.14
30	p	0.012	0.064	0.052	5.3

dow had been less than 0.5 mm thick. Energy loss and remaining range in the carbon targets were estimated with the range tables of Ref. [25] for protons and the relationship $R_d(E) = 2\,R_p(E/2)$. The actual beam energies on targets and ranges were (15.0 MeV, 1.0 mm) at $E_d = 20$ MeV and (26.5 MeV, 2.6 mm) at $E_d = 30$ MeV. Therefore, a large fraction of neutrons was produced in the window and masked the differences of the yields in the target ma-

terials. The observed gain g is written as

$$g = \frac{y_{Al}(E_d) - y_{Al}(E_C) + y_{13}(E_C)}{y_{Al}(E_d) - y_{Al}(E_C) + y_{12}(E_C)}$$

where y's stand for the thick target neutron yields for a deuteron beam of the listed energy, E_d being the beam energy and E_C the energy of the deuteron when it enters the carbon target. The IPN-Orsay group studied neutron yields for various materials including Be, C and U [24], from which a trend is a decrease with Z. An upper limit of the Al-window contribution is therefore obtained by replacing y_{Al} with y_{12C}. The observed ratios y(^{13}C)/y(^{12}C) of 1.17 ($E_d = 20$ MeV) and 1.18 (30 MeV) convert to 1.35 ($E_C = 15$ MeV) and 1.24 (26.5 MeV). The higher gain at lower beam energy is according to the expectation. Yet, the factors remain close to unity and exclude any significant increase of yield.

5.2 Comparison with a Monte-Carlo calculation

A model calculation has been made with the aluminum window and neither represents the full effect of the change of targets, though it applies to a realistic experimental setup and reflects the present experiment.

These calculations were done with the version 2.6.0 of MCNPx, the Monte Carlo N-Particle Transport Code System for Multiparticle and High-Energy Applications, Version 2.6.0 [26]. In the simulation, the deuteron beam has a Gaussian profile with a FWHM of 1.7 mm in both directions normal to the beam axis. It passes through a 0.5 mm thick aluminum foil and is stopped in the target (natural carbon and carbon enriched in ^{13}C of same composition and density as the powder used in the experiment). The neutron flux per steradian and deuteron is obtained by counting the neutrons impinging on 1 cm^2 disks placed at 10 cm from the target and at the experimental angles from the beam axis. The continuous energy spectrum was then binned with a 1 MeV interval in order to obtain the double-differential distribution per MeV, normalised by the solid angle defined by the disks and by the number of incident deuterons.

Table 5 compares the integrals of the experimental and calculated double-distributions per steradian. The experimental values are the integrals of the spectra shown in figures 3, 4, 5 and 6. In both cases the energy cut-off is 1 MeV. The MCNPx calculation is in rather good agreement with the data. It may be meaningful to note a systematical variation of the ratio of calculated and experimental flux with deuteron energy. For natural carbon the flux of neutrons above 4 MeV and up to 50° was overestimated by a factor of 1.45 at $E_d = 40$ MeV [16]. The corresponding factor is 1.07 at $E_d = 30$ MeV and 0.72 (now an underestimation) at 20 MeV. Aside from that too strong variation, the most striking differences are the underestimation of the flux at 0°, and a higher median

Table 5. Experimental and calculated number of neutrons per steradian for 100 deuterons and median energy, at the specified angle θ to the beam axis. The energy threshold is 1 MeV.

E_{med} (MeV), A	n/sr/100 d (θ)		E_{med} (MeV)	
20, ^{12}C	Exper.	MCNPx	Exper.	MCNPx
0°	0.471	0.179	8.4	8.4
20°	0.184	0.118	5.8	8.1
40°	0.078	0.082	3.7	7.4
60°		0.044		5.7
90°	0.018	0.014	2.6	3.6
20, ^{13}C	Exper.	MCNPx	Exper.	MCNPx
0°	0.499	0.181	7.9	8.3
20°	0.225	0.125	4.3	7.9
40°	0.100	0.090	3.3	7.5
60°	0.059	0.047	2.7	5.7
90°	0.041	0.016	2.4	3.4
30, ^{12}C	Exper.	MCNPx	Exper.	MCNPx
0°	1.382	0.822	11.9	12.1
20°	0.417	0.435	7.3	11.1
40°	0.153	0.265	5.8	9.7
60°	0.091	0.113	4.2	7.2
90°	0.065	0.030	3.4	4.1
30, ^{13}C	Exper.	MCNPx	Exper.	MCNPx
0°	1.595	0.860	11.4	12.0
20°	0.490	0.477	6.6	10.8
40°	0.223	0.300	5.2	9.0
60°	0.140	0.131	3.8	6.4
90°	0.096	0.043	3.2	3.2

energy at other angles. A similar situation was observed at a deuteron energy of 40 MeV. The integrated angular distributions come closer to the experimental ones at the largest angles. It appears as if neutrons have been more scattered off-axis in the calculation than they actually were. Yet, the calculation reproduces well the experimental ratio y(^{13}C)/y(^{12}C), being 1.07 (20 MeV), 1.09 (30 MeV) for neutrons within an angle of 30°. The gains appear to be twice less than the experimental ones, but it is little meaningful because of the estimated 8% error on the experimental ratios. More important is confirmation that the gain is small, all ratios being close to one. Both experiment and calculation suggest that the ^{13}C target is not an interesting option for deuteron beams. In both experiment and calculation the gain increases weakly with the angle, but the flux at large angles is small.

6 Summary and outlook

The neutron yield of thick targets of carbon, natural and enriched to 82% in ^{13}C, bombarded with 20 and 30 MeV deuterons has been measured by neutron activation. Agreement with Time-of-Flight measurements for d + ^{12}C re-

ported in the literature shows the results are correct, despite the limited number of usable reactions available to extract the spectra by unfolding the overlaps with the activation cross-sections. The MCNPx code, version 2.6.0, reproduces the experimental distributions fairly well, and especially well the gain obtained with ^{13}C. The most salient and recurrent discrepancy with experiment is the underestimate of the spectrum at 0° which, however, is systematic and not bound to the present experiment. The MCNPx code therefore is suitable to make predictions when both the target and the projectile have a weakly-bound neutron. The ratio of neutron yields of ^{13}C and ^{12}C is modest, being about 1.2, and probably had not even been reaching 1.3 if the 0.5 mm aluminum window did not exist. The small gain hardly can justify the use of the expensive enriched target in a facility where high beam power implies damages and frequent replacement of the neutron-production target, as for instance SPIRAL2 (40 MeV, 5 mA).

A ^{13}C target remains interesting for beams of low-energy protons, where the gain is high, and as long as the deposited power does not require frequent replacement, to say up to few tens of μA. This option is especially worth to consider at a low-energy cyclotron because the maximum beam energy of deuterons is half the maximum energy of protons. Taking the new high-current MCC-30 cyclotron at Jyväskylä as example, the yield read from figure 8 is $0.64\,10^{-3}$ n/p for 30 MeV protons and $0.77\,10^{-3}$ n/d for 15 MeV deuterons. These figures are close to each other and a proton beam may be preferred as it is easier to handle. The selected option indeed is a 30 MeV proton beam on a beryllium target. Neutron yield measurements have been carried out also via the activation method. A yield at 0° of $3\,10^{10}$ n/sr/μC has been observed [27], equivalent to $4.8\,10^{-3}$ n/sr/p. For a ^{13}C target the integrals of distributions extracted from Ref.[15] are $1.6\,10^{-4}$ (E$_p$= 20 MeV), $4.8\,10^{-4}$ (25 MeV) and $2.9\,10^{-3}$ (40 MeV) and the interpolation at 30 MeV results in $1.1\,10^{-3}$ n/sr/p. The yield of the ^{13}C target with 30 MeV protons is therefore 4.4 times lower than the yield of Be. It confirms that beryllium is the best choice for a target as far as its toxicity is not a problem and the geometry of converter and fission target can be made compact, which is possible because the IGISOL target is at low temperature. Finally, at same beam energy for protons and deuterons, which could apply to a linac such as the driver of SPIRAL2, deuteron beams remain the best choice. The integral of the spectrum at 0° in figure 6 gives $1.6\,10^{-2}$ n/sr/d, still 3.3 times more than for protons on beryllium.

7 Acknowledgments

References

1. ISOLDE, the radioactive beam facility, isolde.web.cern.ch/.
2. T. Stora, E. Noah, R. Hodak, T.Y. Hirsh, M. Hass, V. Kumar, K. Singh, S. Vaintraub, P. Delahaye, H. Frånberg-Delahaye, M.-G. Saint-Laurent, G. Lhersonneau, Europhys. Lett. **98**, 32001 (2012) 32001.
3. I.D. Moore, T. Eronen, D. Gorelov, J. Hakala, A. Jokinen, A. Kankainen, V.S. Kolhinen, J. Koponen, H. Penttilä, I. Pohjalainen, M. Reponen, J. Rissanen, A. Saastamoinen, S. Rinta-Antila, V. Sonnenschein, J. Äystö, Nuclear Inst. and Methods in Physics Research B **317**, (2013) 208.
4. Y. Blumenfeld and G. Fortuna, *A design study for a European Isotope Separation On-Line Radiaoactive Beam Facility*, (edited by J. Cornell, GANIL, Caen, France, November 2009) and http://www.ganil-spiral2.eu/eurisol.
5. S. Galès, Nuclear Physics A **834**, (2010) 717, and http://www.ganil-spiral2.eu/.
6. X. Ledoux, M. Aïche, M. Avrigeanu, V. Avrigeanu, L. Audouin, E. Balanzat, B. Ban-d'État, G. Ban, G. Barreau, E. Bauge, et al., AIP Conf. Proc. *1412*, (2011) 55 and Nuclear Data Sheets **119** (2014) 353.
7. C. Gustavsson, S. Pomp, G. Scian, F.R. Lecolley, U. Tippawan and Y. Watanabe, Physica Scripta **2012**, (2012) T150.
8. ARCHADE, Advanced Resource Center for HADrontherapy in Europe, http://www.france-hadron.fr/fr/noeuds/archade-caen.html.
9. F. Minato and Y. Nagai, J. Phys. Soc. Japan **79** (2010) 093201.
10. IFMIF, International Fusion Materials Irradiation Facility, www.frascati.enea.it/ifmif/
11. ITER, International Thermonuclear Experimental Reactor, www.iter.org/
12. National Nuclear Data Center, https://www.nndc.bnl.gov.
13. A. Bracco and A. Pisent; (LNL-INFN(REP) 181/02, Legnaro, Italy, 2002), http://www.lnl.infn.it/ spes/
14. O. Alyakrinskiy, A. Andrighetto, M. Barbui, S. Brandenburg, M. Cinausero, B. Dalena, P. Dendooven, E. Fioretto, G. Lhersonneau, W. Lyapind, G. Prete, G. Simonetti, L. Stroe, L.B. Tecchio, W.H. Trzaska, Nuclear Inst. and Methods in Physics Research A, **547**, (2005) 616.
15. G. Lhersonneau, T. Malkiewicz, D. Vakhtin, V. Plockhoi, O. Alyakrinskiy, C. Cinausero, Ya. Kandiev, H. Kettunen, S. Khlebnikov, H. Penttilä, G. Prete, V. Rizzi, S. Samarin, L. Teccchio, W.H. Trzaska, and G. Tyurin, Nuclear Inst. and Methods in Physics Research A **576**, (2007) 371.
16. G. Lhersonneau, T. Malkiewicz, K. Kolos, M. Fadil, H. Kettunen, M.G. Saint-Laurent, A. Pichard, W.H. Trzaska, G. Tyurin, L. Cousin, Nuclear Inst. and Methods in Physics Research A **603**, (2009) 228.

17. G. Lhersonneau, T. Malkiewicz, P. Jones, S. Ketelhut and W.H. Trzaska, Eur. Phys. J. A **48**, (2012) 116.
18. G. Lhersonneau, T. Malkiewicz, P. Jones, P. Karvonen, S. Ketelhut, O. Bajeat, M. Fadil, S. Gaudu, M.G. Saint-Laurent, W.H. Trzaska, Nuclear Inst. and Methods in Physics Research A **698**, (2013) 224.
19. G. Lhersonneau, T. Malkiewicz, W.H. Traska, Hyp. Interactions **223**, (2014) 253, DOI: 10.1007/s10751-012-0612-9 (2012).
20. A. Donzella, M. Barbui, F. Bocci, G. Bonomi, M. Cinausero, D. Fabris, A. Fontana, E. Giroletti, M. Lunardon, S. Moretto, G. Nebbia, M.M. Necchi, S. Pesente, G. Prete, V. Rizzi, G. Viesti, A. Zenoni, Nuclear Inst. and Methods in Physics Research A **6**13, (2010) 58.
21. Keithley 6485 Picoammeter, http://www.keithley.com/products/dcac/sensitive/lowcurrent?mn=6485.
22. Goodfellow, www.goodfellow.com.
23. X-ray attenuation coefficients tables, http://www.nist.gov/pml/data/xraycoef/index.cfm.
24. N. Pauwels, F. Clapier, J. Proust, M. Mirea, hhttp://www.nea.fr/html/science/satif/satif5_pauwels.pdfi, and N. Pauwels, Ph.D. Thesis, IPN-Orsay, IPNO-T-00-12, 2000.
25. Range and stopping power calculator, http://www.nist.gov/pml/data/star/index.cfm.
26. Monte Carlo N-Particle Transport Code System for Multiparticle and High Energy Applications, Version 2.6.0 (November 2007), Oak Ridge National Laboratory (ORNL/RSICC), USA, 2007.

27. D. Gorelov, Nuclear fisssion studies with the IGISOL method and JYFLTRAP, PhD University of Jyväskylä, 2015, Department of Physics Research Report, No. 12/2015.